LAR detection for On-Orbit Servicing: Performance Analysis of Classical Approaches, Failure Modes and Mitigation Strategies

1st Supuni Kaveendya Kirimamuni
SpaceR/SNT
University of Luxembourg
Kirchberg, Luxembourg
supuni.kirimamuni@uni.lu

2nd Lina Amaya-Mejia
SpaceR/SNT
University of Luxembourg
Kirchberg, Luxembourg
lina.amaya@uni.lu

3rd Carol Martinez
SpaceR/SNT
University of Luxembourg
Kirchberg, Luxembourg
carol.martinezluna@uni.lu

***Abstract*—Reliable perception of a target is essential in robotic on-orbit servicing (OOS) tasks, where a servicer must localize and approach a target spacecraft under visually challenging conditions caused by harsh space environments. This paper presents a performance analysis of classical edge-based detection methods for LAR detection, analysis of observed failure modes, and mitigation strategies. Sobel, Canny, and Laplacian-of-Gaussian (LoG) edge detectors are evaluated within a unified perception pipeline along with a failure study, review of mitigation strategies, and recommendation of the most computationally efficient approach. Extensive experiments on representative datasets reveal high overall robustness of edge-based methods, with the proposed pipeline achieving an average detection accuracy of 0.94 for inner and outer rings (Canny: 1.00, LoG: 0.85, Sobel: 0.92), yet also expose distinct failure modes under harsh illumination and false detections due to satellite body clutter or reflections. We review existing strategies in classical and deep learning based on addressing observed failures, considering computational constraints in space applications.**

***Index Terms*—Launch Adapter ring(LAR), Edge Detection, On-Orbit Servicing(OOS),Illumination Robust**

Fig. 1. Simulated orbital scenario of a servicer approaching a target satellite [2]

I. Introduction

Autonomous on-orbit servicing (OOS) missions (orbital refueling, satellite repairing, and assembly) have become the foundation of sustainable space operations. Visuomotor skills can enhance OOS operations by tracking objects, navigating through complex and dynamic environments, and improving precision, flexibility, and robustness during critical OOS missions. Visuomotor skills are acquired through visual perception strategies that allow the robot to approach, grasp, and manipulate objects by controlling the relative motion of the robot based on visual observations [1]. In the context of OOS, target satellites present several structural geometric landmarks that can be exploited for vision-based perception, such as antennas, nozzles, solar panels, and the launch adapter ring (LAR). Among these, solar panels are relatively easy to detect due to their large surface area; however, most satellite components are predominantly rectangular in shape, and solar panels themselves are thin and mechanically fragile. In contrast, the LAR is a critical structural interface common to most satellites, large in size, rigid, and well-defined, with sharp, easily detectable edges [3] [4] [5]. Its circular geometry provides a distinct and symmetrical shape that is well-suited for reliable visual identification. Furthermore, its metallic surface enhances reflectivity, improving edge detection based on image gradient variations. These characteristics make the LAR an ideal target for both detection and robotic grasping. However, due to unfavorable conditions in the space environment, the perception of such structures poses a unique challenge [1]. These include extreme lighting variations, reflectivity of the target's surface, ineffectiveness during eclipse, low signal-to-noise ratio, inferior sensor resolution [6], uncertainty, and limited processing power [7], which degrade the image features and affect the real-time performance of the system [1].

To study these challenges and how existing algorithms behave under these conditions, this research conducts a comparative performance analysis of classical CV algorithms integrated into a unified perception pipeline for reliable detection of LAR. This work focuses on quantitative benchmarking of edge detection algorithms to provide insights into their

accuracy by using metrics such as circularity, residual fit error, and processing latency to characterize detection performance , computational efficiency and their limitations. Furthermore, failure modes are systematically identified and analyzed, and corresponding mitigation strategies are explored to enhance robustness under challenging conditions.

The key contributions of this work are:

- A comparative performance analysis of classical edge detection algorithms **Sobel, Laplacian of Gaussian(LoG), Canny** applied to image sequences of Launch Adaptor Rings, assessing relative accuracy, and computational efficiency.
- **A study of observed failure modes** in LAR detection, including false detection, and sensitivity to illumination variations.
- An evaluation of existing **classical and hybrid mitigation strategies** with explicit focus on the trade-off between **detection robustness and computational efficiency.**

II. Related Work

Detection of LAR has been explored for robotic OOS for capture and servicing operations. Most work employees either Canny [8] or Sobel [9] edge detection algorithms come in the classical computer vision world. Several studies [10] [11] [12] [13] [14], used the Canny operator to extract the edges of the circular LAR, and once the edges are extracted, contour-based methods are used to detect the LAR considering facts as convexity, gradient direction, and polygonal approximation. Also, following the same procedures, Xu et al. [15] detected edges and used randomized Hough transform (RHT) to detect the ellipses.

Velasquez et al. [16] did an experimental evaluation of a vision-based system for pose estimation. This work is performed on the blue channel, yielding better contrast between the ring and the insulation layer. They also used the Canny detector for image edges extraction, from edge map, Its feature extraction is done by using modified version of FastEllipseExtraction(FEE) to locate potential arcs and ellipses. And using FitEllipse the ellipses that best fit the known size and position of the LAR is computed and comparing the cost function to score and ellipse with lowest score is selected as the ring. Liu et al. [17] proposes a vision-based approach to detect the LAR and compute the pose estimation. Their method begins with using sobel operator to edge detection and then length-based line segment detector that extracts piecewise-linear segments from images, preserving essential geometric shapes like ellipses while reducing data volume. This is followed by a robust ellipse detection algorithm that handles partial ellipses through edge fragment searching and contour re-finding, demonstrating resilience to outliers, noise, and occlusions. Zhan et al. [12] proposes a method for detecting and pose estimation of LAR using neural networks and supervised learning addressing the ambiguity. Key concept is to breaking circle into uneven 3d points to break symmetry. This detects the LAR and using NN RestNet as backbone feature extractor, detects the ring area by semantic mask making a bounding box.

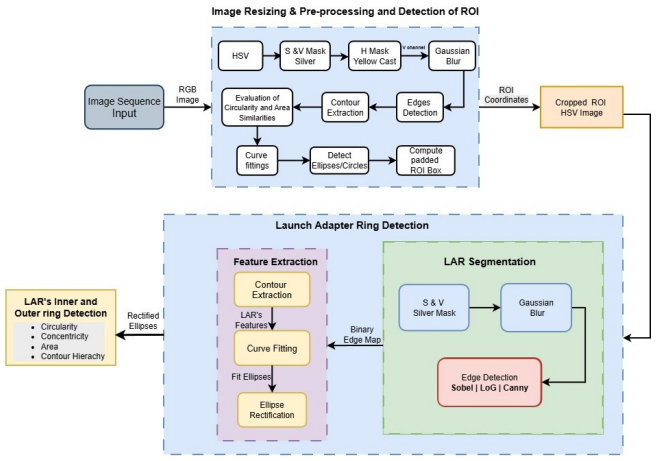

Fig. 2. Block diagram of proposed solution for detecting the LAR.

Overall, the classical approach of detecting the LAR are very reliable and most used. However they are not 100% accurate. This paper performs a comparative analysis between these methods and observes failure scenarios and studies existing strategies to mitigate these failures.

III. Launch Adapter Ring Detection - The Proposed Solution

In this paper, we propose a vision-based fully classical geometry-driven method to robustly detect the outer and inner ring structures of the LAR based on the gradient direction of edges and evaluate different state-of-the-art edge detection operators, Sobel, LoG, and Canny, under different illuminations, angles, and distances. The top block of Fig 2 describes the proposed classical pipeline of detection of LAR through each stage of the pipeline, which consists of: (a) image resizing, pre-processing, and detection of ROI, (b) segmentation of the LAR (c) LAR's feature extraction and ellipse fitting and (d) detection of the LAR.

A. Image Resizing, Pre-processing and ROI Detection

To reduce the computational cost, we first downscaled the input RGB image by 400% and focused taking a region of interest (ROI). And then the image containing ROI converted into HSV. A silver region mask is applied using low-S and high-V colors space thresholding to isolate metallic silver areas and to increase the robustness to gold-foil MLI reflections yellow metallic hues (H) are added to the mask.

$$H_y \in [15^\circ, 40^\circ], \quad S_y \in [30, 120], \quad V_y \in [80, 255]$$

A binary mask,

$$M(p) = M_{\text{silver}}(p) \ \vee \ M_{\text{yellow}}(p)$$

is obtained by combining the silver and yellow masks. The resulting mask is subjected to morphological opening and closing to remove small artifacts while preserving larger curved structures. The masked image is then smoothed using a 5 X 5

Gaussian kernel to suppress noise. Using the detected metallic colors as priors, candidate contours are analyzed based on circularity and approximate size, enabling the estimation of a coarse bounding box around ring-like structures. This bounding box defines a high-confidence ROI. Once the ROI is identified, the algorithm isolates the LAR by focusing on the metallic structures within this cropped region.

B. LAR's Feature Extraction

The LAR has reflective properties that differ from the surrounding background, resulting in a sharp change in image brightness and intensity [11]. Hence, edge pixels are extracted to determine the boundary of the ring by applying the Canny edge detector [18] to the masked image with thresholds derived from local image intensity values. This produces a binary edge map containing potential ring boundaries.

From the edge map, the contours are extracted using hierarchical tree-structured retrieval `findContours(RETR_TREE)` [19] that detects parent-child relationships between the nested structure of the identified contours. This is an important feature for distinguishing inner and outer rings. The contour filtering to eliminate noise and irrelevant features is done using the following criteria:

- It takes at least 5 points to fit an ellipse. So, the number of points should be > 5.
- Minimum area A should be at least $\geq 0.02\%$ of ROI – to remove the spurious detections.
- The number of vertices of the polygon must be ≥ 6 by Douglas–Peucker polygonal approximation [20] to ensure that only sufficiently smooth, curved shapes are kept.
- **Circularity** (C) is computed.

$$C = \frac{4\pi A}{P^2} \tag{1}$$

Once all criteria are met, shape similarity is assessed using Hu moment invariants [21], integrated into the score as filtered contours are furthermore scored by combining area and circularity. Circularity Score is computed to rank all the ring candidates.

$$CS = \frac{C * A}{\text{Shape Similarity}} \tag{2}$$

The contour with highest score is selected as the **outer ring candidates.**

The inner ring is extracted via following up the hierarchical feature of the contour. The algorithm applies to all the children-contours of the outer ring. For each potential contour, the algorithm checks:

- **Scale ratio**, ensuring the inner ring area is between 20–80% of the outer ring.
- **Center displacement:**

$$d = \sqrt{(c_{x,\text{cand}} - c_{x,\text{ref}})^2 + (c_{y,\text{cand}} - c_{y,\text{ref}})^2} \leq 10$$

pixels, ensuring both ellipses are nearly concentric.

Out of all the valid contours, the contour with the highest circularity score is selected as **inner ring** contour.

C. Ellipse Fitting and validation

Ellipses are fitted for the selected inner and outer ring candidates using cv2.fitEllipseAMS [22] using direct least-squares [23] minimization, solving the conic expression of the ellipse, and then acquiring 5D parameters of the ellipses as:

$$Ax^2 + Bxy + Cy^2 + Dx + Ey + F = 0 \tag{3}$$

This algebraic approach minimizes the squared residuals

$$\sum (Ax_i^2 + Bx_iy_i + Cy_i^2 + Dx_i + Ey_i + F)^2$$

via eigenvalue decomposition of the design matrix, providing a non-iterative, stable fit robust to noise [23].

Further validation is done on the selected inner and outer rings, by reference ellipses are fitted using the above method and taking geometric parameters: center c_xc_y, major/minor axes a, b, and rotation angle θ. These parameters serve as reference to quantify detection performance. Key validation metrics are as follows:

- **Axis ratio similarity:**

$$|(a/b)_{\text{cand}} - (a/b)_{\text{ref}}| \leq 0.1$$

- **Area ratio for inner–outer pairs:**

$$k \in [0.2, 0.8], \quad \text{candidate } k \text{ within } 5\% \text{ of reference } k$$

The intermediate processing results of the proposed pipeline are illustrated in Fig 3.

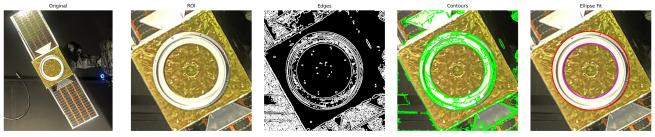

Fig. 3. Intermediate processing results of the detection pipeline of LAR

IV. Experiments and Results

A. Experimental Setup

To assess the performance of the proposed algorithm, tests were performed on real image sequence. The general experimental setup is illustrated in Fig. 4. The setup consists of a chaser robotic manipulator (UR10) equipped with an end-effector camera and a satellite mockup mounted on a second UR arm that follows a predefined 6-DoF trajectory. The mockup replicates a real non-cooperative satellite with a 30 cm × 30 cm × 30 cm cube covered in MLI, an attached Launch Adapter Ring (25 cm diameter and 27 cm thickness), and two solar panels.

The algorithm is implemented in Python and executed on a laptop running Windows 11, equipped with a NVIDIA RTX 3080 GPU and 16 GB of RAM.

Fig. 4. Experimental setup at the Zero-G Lab, University of Luxembourg.

B. Testing Procedure

In addition to the validation steps done in section III, subsection C, there are few tests have been carried out in analyzing the detection accuracy. Ground truth annotations were used to compute quantitative performance metrics for each edge detection algorithm as well. The detected outputs were compared with the annotated reference data to measure detection accuracy, robustness, and consistency across the images.

C. Results

Figures 5 show the edge map obtained from the edge detection algorithms and clearly visible differences,and 6 show outputs of the detected rings from the evaluated algorithms.

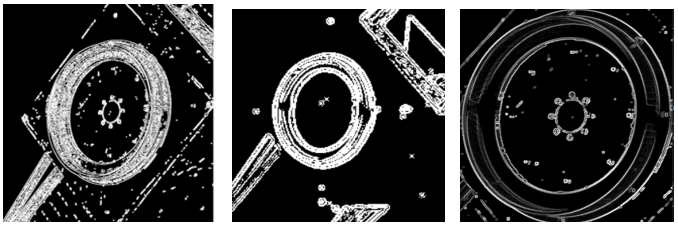

(a) **Canny** (b) **LoG** (c) **Sobel**

Fig. 5. Edge maps of evaluated algorithms.

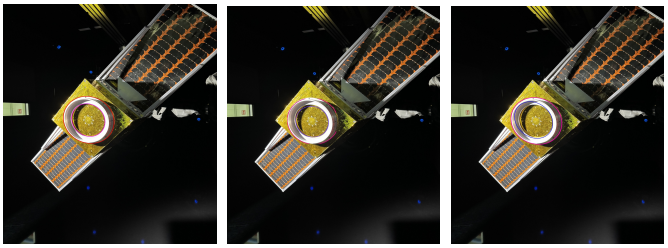

(a) **Canny** (b) **LoG** (c) **Sobel**

Fig. 6. Detection results from the three evaluated algorithms.

The following graph presents the comparison of the detection accuracy results achieved by each algorithm, demonstrating that canny achieved the highest accuracy in detecting both rings.

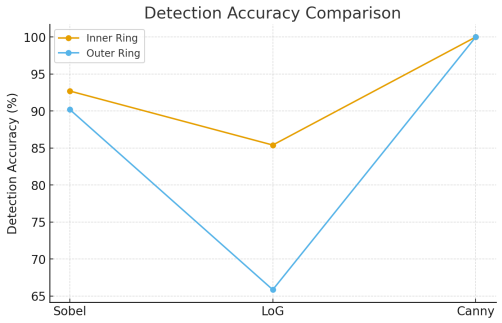

Fig. 7. Detection accuracy comparison across three algorithms

V. Failure Mode Analysis and Mitigation Strategies

A. Failure Modes

The study revealed a few distinct failure scenarios when detecting LAR using classical edge detection methods. One specific scenario is when the LAR is under high illumination, due to direct exposure of the sunlight on surface as well as reflected off the solar panels,leading to additional glare and intensified brightness. LAR boundaries suffer from severe contrast reduction, specular reflections, and saturation effects, leading to significant degradation in edge detection performance. Therefore, the pipeline fails to detect the rings. The primary failures observed include:

- Missed edges due to low local contrast caused by sensor saturation and washed-out gradients.
- Fragmented or discontinuous edge segments along LAR boundaries.
- Increased false negatives at highlight regions where intensity clipping occurs.

The analyzed representative failure cases are shown in Figure 8, which presents the ground truth (a) annotation alongside a correctly localized LAR, serving as a reference for expected performance. In contrast, the subsequent examples (b & c) highlight failure scenarios where the method produced false detections, struggles to extract continuous edge structures, or fails to detect the LAR entirely.

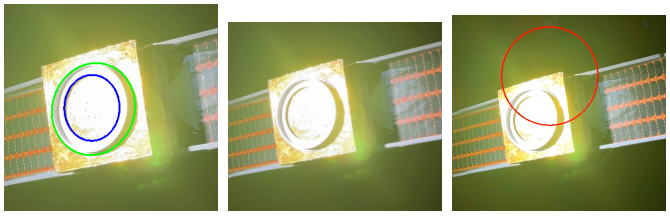

(a) **GT** (b) Failed Scenario 1 (c) Failed Scenario 2

Fig. 8. Failure scenario comparison with the GT

B. Mitigation strategies

Several mitigation strategies were explored, from which two approaches emerged as the most effective. These methods are

evaluated to address failures under high illumination while prioritizing computational efficiency for space systems. Both approaches maintained the subsequent feature extraction and ellipse fitting stages of the original pipeline.

1) Classical Approach: A channel-wise analysis was first performed to identify the most robust color channel for edge extraction. The blue channel was selected due to its superior contrast characteristics and lower susceptibility to saturation under intense illumination [16]. This choice enhances the visibility of structural boundaries in LARs and stabilizes downstream feature extraction. To overcome the fundamental limitations of gradient-based detectors (which are highly sensitive to illumination variations), the edge detection step was replaced with a phase congruency [24] based method. Unlike conventional approaches that rely on intensity gradients, phase congruency detects features based on the alignment of local frequency components across multiple scales and orientations. This results in a dimensionless measure of feature significance that is invariant to changes in image contrast and illumination.

2) Hybrid Approach : As the second strategy, a hybrid method was investigated that combines deep learning take ROI with classical edge detection within the region of interest (ROI). A lightweight YOLOv8n [25] model was employed to generate a tight bounding box around the target rings, enabling accurate ROI extraction. Within this cropped region, the proposed classical pipeline replacing canny operator with phase congruency was applied.

Representative results of both approaches on challenging high-illumination images are presented in Figure 9. Both

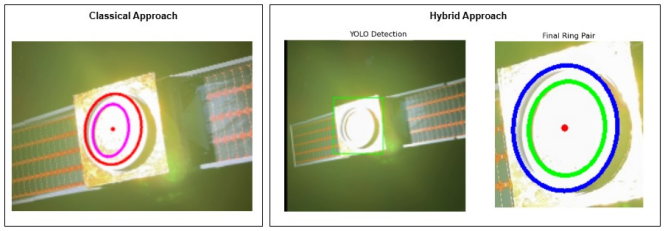

Fig. 9. Detection results of LAR in failed scenarios

mitigation strategies achieved excellent detection accuracy, successfully identifying both rings in 98% of the tested high-illumination cases. However, computational cost remains a critical constraint for onboard space applications. The classical phase-congruency approach required approximately 221.5 ms for edge detection alone and 265 ms for the complete pipeline per image. In contrast, the hybrid approach was significantly faster, with an average breakdown of 8.6 ms for pre-processing, 68.9 ms for YOLOv8n inference, and 132.9 for the whole pipeline, resulting in a total processing time less than half that of the classical method. The following graph in figure 10 shows the accuracy vs computational cost trade-off. Given the stringent processing power limitations typical of space systems, the hybrid approach offers a compelling trade-off. It delivers comparable robustness while substantially reducing computational demand, making it more suitable

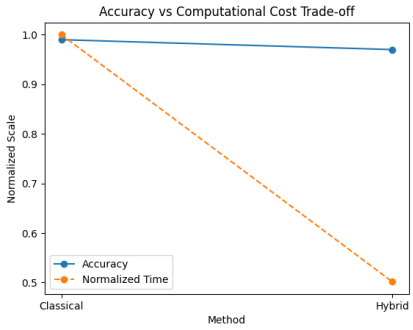

Fig. 10. Accuracy vs. computational cost trade-off for classical and hybrid approaches

for real-time or near-real-time LAR detection in resource-constrained environments.

VI. Conclusion

This work presented a visual perception pipeline for LAR detection under challenging space imaging conditions, including a comparative evaluation of classical edge detection methods and a failure analysis. Among the evaluated original edge detection approaches, Canny demonstrated the most reliable detection performance, while Sobel offered a favorable trade-off between accuracy and computational cost, and LoG proved unsuitable due to low accuracy and higher computational cost.

The analysis shows that gradient-based methods are inherently limited due to their reliance on intensity variations, which leads to failures under low-contrast and harsh illumination conditions. Failure analysis further revealed that detection performance is strongly dependent on accurate ROI localization,when the ROI is correctly identified, the LAR can be detected reliably even under challenging scenarios. In this context, YOLO-based ROI extraction provides more consistent and robust results by effectively constraining the search space.

Additionally, phase congruency improves robustness in difficult lighting conditions being illumination invariant, while the hybrid approach offers a practical balance between detection accuracy and computational efficiency. Future work will focus on reducing the computational cost of classical methods and exploring fully deep learning-based approaches to achieve robust performance across varying illumination conditions.

References

[1] L. M. Amaya-Mejía, M. Ghita, J. Dentler, M. Olivares-Mendez, and C. Martinez, "Visual servoing for robotic on-orbit servicing: A survey," in *2024 International Conference on Space Robotics (iSpaRo)*. IEEE, Jun. 2024, p. 178–185. [Online]. Available: http://dx.doi.org/10.1109/iSpaRo60631.2024.10687516

[2] I. Hatty, "Viability of on-orbit servicing spacecraft to prolong the operational life of satellites," *Journal of Space Safety Engineering*, vol. 9, no. 2, pp. 263–268, 2022. [Online]. Available: https://www.sciencedirect.com/science/article/pii/S2468896722000131

[3] D. Zhang, G. Yang, J. Ji, S. Fan, M. Jin, and H. Liu, "Constrained visual servoing for capturing adapter rings on tumbling satellites with a free-floating robot," *IEEE Transactions on Aerospace and Electronic Systems*, vol. 61, no. 3, pp. 6026–6040, 2025.

[4] C. G. Henshaw, S. Glassner, B. Naasz, and B. Roberts, "Grappling spacecraft," *Annual Review of Control, Robotics, and Autonomous Systems*, vol. 5, pp. 267–296, 2022.

[5] K. Fujii, I. Rodríguez, M. Schedl, G. Grunwald, and M. A. Roa, "Comparative analysis of robotic gripping solutions for cooperative and non-cooperative targets," in *2024 IEEE Aerospace Conference*, 2024, pp. 1–14.

[6] B. Candan and S. Servadio, "Markers identification for relative pose estimation of an uncooperative target," 2024. [Online]. Available: https://arxiv.org/abs/2407.20515

[7] F. Sellmaier, T. Boge, J. Spurmann, S. Gully, T. Rupp, and F. Huber, *On-Orbit Servicing Missions: Challenges and Solutions for Spacecraft Operations*. [Online]. Available: https://arc.aiaa.org/doi/abs/10.2514/6.2010-2159

[8] J. Canny, "A computational approach to edge detection," *IEEE Transactions on Pattern Analysis and Machine Intelligence*, vol. 8, pp. 679–698, 1986.

[9] O. Vincent and O. Folorunso, "A descriptive algorithm for sobel image edge detection," 01 2009.

[10] G. D'Amico, "6dof pose estimation for space applications," Master's thesis, Politecnico di Torino, Turin, Italy, 2021. [Online]. Available: https://webthesis.biblio.polito.it/19121/

[11] L. Zhang, W. Pan, and X. Ma, "Real-time docking ring detection based on the geometrical shape for an on-orbit spacecraft," *Sensors*, vol. 19, no. 23, 2019. [Online]. Available: https://www.mdpi.com/1424-8220/19/23/5243

[12] W. Zhang, P. Xiao, and J. Li, "Satellite pose estimation via only a single spatial circle," *Information*, vol. 13, no. 2, 2022. [Online]. Available: https://www.mdpi.com/2078-2489/13/2/95

[13] L. Tingting, D. Zhijun, G. Xin, F. Zhiting, W. Xinfeng, and W. Hua, "An ellipse detection algorithm for spacecraft optical navigation," *Journal of Beijing University of Aeronautics and Astronautics*, vol. 49, no. 4, pp. 853–868, 2023. [Online]. Available: https://bhxb.buaa.edu.cn/bhzk/en/article/doi/10.13700/j.bh.1001-5965.2021.0363

[14] Y. Liu, Z. Xie, B. Wang, and H. Liu, "Pose measurement of a non-cooperative spacecraft based on circular features," in *2016 IEEE International Conference on Real-time Computing and Robotics (RCAR)*, 2016, pp. 221–226.

[15] W. Xu, Q. Xue, H. Liu, X. Du, and B. Liang, "A pose measurement method of a non-cooperative geo spacecraft based on stereo vision," in *2012 12th International Conference on Control Automation Robotics & Vision (ICARCV)*, 2012, pp. 966–971.

[16] A. F. Velasquez, J. Luckett, M. Napolitano, G. Marani, T. Evans, and M. Fravolini, *Experimental Evaluation of a Machine Vision Based Pose Estimation System for Autonomous Capture of Satellites with Interface Rings*. [Online]. Available: https://arc.aiaa.org/doi/abs/10.2514/6.2013-4758

[17] Y. Liu, Z. Xie, Q. Zhang, X. Zhao, and H. Liu, "A new approach for the estimation of non-cooperative satellites based on circular feature extraction," *Robotics and Autonomous Systems*, vol. 129, p. 103532, 2020. [Online]. Available: https://www.sciencedirect.com/science/article/pii/S0921889019307158

[18] J. Canny, "A computational approach to edge detection," *IEEE Transactions on Pattern Analysis and Machine Intelligence*, vol. PAMI-8, no. 6, pp. 679–698, 1986.

[19] S. Suzuki and K. Abe, "Topological structural analysis of digitized binary images by border following," *Comput. Vis. Graph. Image Process.*, vol. 30, pp. 32–46, 1985. [Online]. Available: https://api.semanticscholar.org/CorpusID:205113350

[20] D. H. DOUGLAS and T. K. PEUCKER, "Algorithms for the reduction of the number of points required to represent a digitized line or its caricature," *Cartographica*, vol. 10, no. 2, pp. 112–122, 1973. [Online]. Available: https://doi.org/10.3138/FM57-6770-U75U-7727

[21] M.-K. Hu, "Visual pattern recognition by moment invariants," *IRE Transactions on Information Theory*, vol. 8, no. 2, pp. 179–187, 1962.

[22] A. Fitzgibbon and R. Fisher, "Direct least square fitting of ellipses," *IEEE Transactions on Pattern Analysis and Machine Intelligence*, vol. 21, 11 2000.

[23] A. Fitzgibbon, M. Pilu, and R. Fisher, "Direct least square fitting of ellipses," *IEEE Transactions on Pattern Analysis and Machine Intelligence*, vol. 21, no. 5, pp. 476–480, 1999.

[24] P. D. Kovesi, "MATLAB and Octave functions for computer vision and image processing," available from: <https://www.peterkovesi.com/matlabfns/>.

[25] G. Jocher, A. Chaurasia, and J. Qiu, "Ultralytics yolov8," 2023. [Online]. Available: https://github.com/ultralytics/ultralytics